ISSN 2277-2685

IJESR/December. 2019/ Vol-9/Issue-4/39-60

ENHANCING DISTRIBUTED POWER MANAGEMENT IN INTERCONNECTED AC/DC MICROGRIDS, PARTICULARLY UNDER UNBALANCED CONDITIONS

B. Esleru Rani[*1], K. Katyayani[*2], M. Ravindnanath[*3]

[*1, 2, 3] Assistant Professor, Dept. of Electrical and Electronics Engineering.

A.M Reddy Memorial College of Engineering and Technology, Andhra Pradesh.

Abstract: This paper introduces a hybrid AC/DC microgrid aimed at streamlining the conversion processes within individual AC or DC grids, thereby minimizing the need for multiple DC–AC–DC or AC–DC–AC conversions. The hybrid grid integrates both AC and DC networks through multi-bidirectional converters, with AC sources and loads linked to the AC network and DC sources and loads connected to the DC network. Energy storage systems can be integrated into either the DC or AC links. The proposed hybrid grid offers flexibility to operate in either grid-tied or autonomous modes. Coordination control algorithms are devised to facilitate seamless power transfer between AC and DC links and to ensure stable system operation across diverse generation and load scenarios. The control strategies account for uncertainties and intermittencies associated with variables such as wind speed, solar irradiation level, ambient temperature, and load fluctuations. A small-scale hybrid grid model is developed and simulated using Simulink in MATLAB. Simulation results demonstrate the system's ability to maintain stable operation under the proposed coordination control strategies during transitions between different operating conditions.

Keywords : AC/DC Microgrids, Power Distribution, Controlled Algorithm.

INTRODUCTION

Three phase ac power systems have existed for over 100 years due to their efficient transformation of ac power at different voltage levels and over long distance as well as the inherent characteristic from fossil energy driven rotating machines. Recently more renewable power conversion systems are connected in low voltage ac distribution systems as distributed generators or ac micro grids due to environmental issues caused by conventional fossil fueled power plants. On other hand, more and more dc loads such as light-emitting diode (LED) light sand electric vehicles (EVs) are connected to ac power systems to save energy and reduce CO emission. When power can be fully supplied by local renewable power sources, long distance high voltage transmission is no longer necessary. AC micro grids have been proposed to facilitate the connection of renewable power sources to conventional ac systems. However, dc power from photovoltaic (PV) panels or fuel cells has to be converted into ac using dc/dc boosters and dc/ac inverters in order to connect to an AC grid.

Wind Energy

Wind power:

Wind is abundant almost in any part of the world. Its existence in nature caused by uneven heating on the surface of the earth as well as the earth's rotation means that the wind resources will always be available. The conventional ways of generating electricity using non renewable resources such as coal, natural gas, oil and so on, have great impacts on the environment as it contributes vast quantities of carbon dioxide to the earth's atmosphere which in turn will cause the temperature of the earth's surface to increase, known as the green house effect. Hence, with the advances in science and technology, ways of generating electricity using renewable energy resources such as the wind are developed. Nowadays, the cost of wind power that is connected to the grid is as cheap as the cost of generating electricity using coal and oil. Thus, the increasing popularity of green electricity means the demand of electricity produced by using non renewable energy is also increased accordingly.

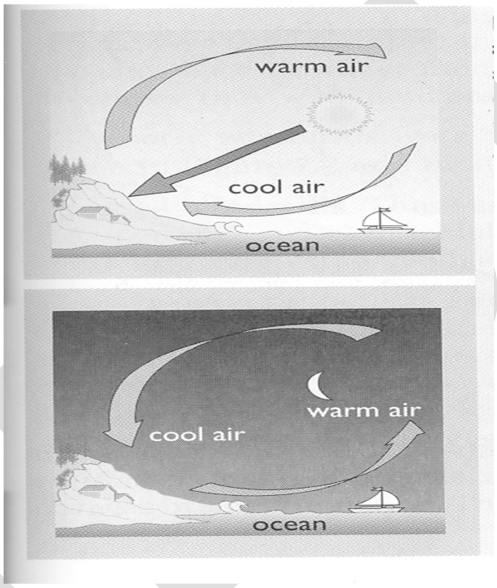

Fig: Formation of wind due to differential heating of land and sea

PHOTOVOLTAIC TECHNOLOGY

Photovoltaic's is the field of technology and research related to the devices which directly convert sunlight into electricity using semiconductors that exhibit the photovoltaic effect. Photovoltaic effect involves the creation of voltage in a material upon exposure to electromagnetic radiation.

The photovoltaic effect was first noted by a French physicist, Edmund Becquerel, in 1839, who found that certain materials would produce small amounts of electric current when exposed to light. In 1905, Albert Einstein described the nature of light and the photoelectric effect on which photovoltaic technology is based, for which he later won a Nobel prize in physics. The first photovoltaic module was built by Bell Laboratories in 1954. It was billed as a solar battery and was mostly just a curiosity as it was too expensive to gain widespread use. In the 1960s, the space industry began to make the first serious use of the technology to provide power aboard spacecraft. Through the space programs, the technology advanced, its reliability was established, and the cost began to decline. During the energy crisis in the 1970s, photovoltaic technology gained recognition as a source of power for non-space applications.

The solar cell is the elementary building block of the photovoltaic technology. Solar cells are made of semiconductor materials, such as silicon. One of the properties of semiconductors that makes them most useful is that their conductivity may easily be modified by introducing impurities into their crystal lattice. For instance, in the fabrication of a photovoltaic solar cell, silicon, which has four valence electrons, is treated to increase its conductivity. On one side of the cell, the impurities, which are phosphorus atoms with five valence electrons (n-donor), donate weakly bound valence electrons to the silicon material, creating excess negative charge carriers.

On the other side, atoms of boron with three valence electrons (p-donor) create a greater affinity than silicon to attract electrons. Because the p-type silicon is in intimate contact with the n-type silicon a p-n junction is established and a diffusion of electrons occurs from the region of high electron concentration (the n-type side) into the region of low electron concentration (p-type side). When the electrons diffuse across the p-n junction, they recombine with holes on the p-type side.

However, the diffusion of carriers does not occur indefinitely, because the imbalance of charge immediately on either sides of the junction originates an electric field. This electric field forms a diode that promotes current to flow in only one direction.

Ohmic metal-semiconductor contacts are made to both the n-type and p-type sides of the solar cell, and the electrodes are ready to be connected to an external load. When photons of light fall on the cell, they transfer their energy to the charge carriers. The electric field across the junction separates photo-generated positive charge carriers (holes) from their negative counterpart (electrons). In this way an electrical current is extracted once the circuit is closed on an external load.

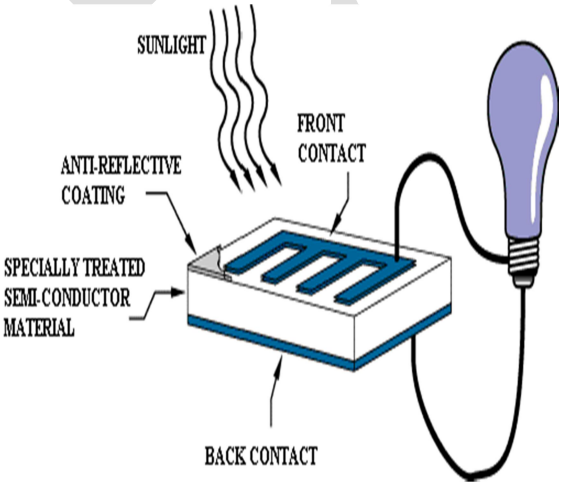

SOLAR CELL

The photovoltaic effect was first reported by Edmund Becquerel in 1839 when he observed that the action of light on a silver coated platinum electrode immersed in electrolyte produced an electric current. Forty years later the first solid state photovoltaic devices were constructed by workers investigating the recently discovered photoconductivity of selenium. In 1876 William Adams and Richard Day found that a photocurrent could be produced in a sample of selenium when contacted by two heated platinum contacts. The photovoltaic action of the

selenium differed from its photoconductive action in that a current was produced spontaneously by the action of light.

No external power supply was needed. In this early photovoltaic device, a rectifying junction had been formed between the semiconductor and the metal contact. In 1894, Charles Fritts prepared what was probably the first large area solar cell by pressing a layer of selenium between gold and another metal.

DC-DC CONVERTER BASICS

A DC-to-DC converter is a device that accepts a DC input voltage and produces a DC output voltage. Typically the output produced is at a different voltage level than the input. In addition, DC-to-DC converters are used to provide noise isolation, power bus regulation, etc. This is a summary of some of the popular DC-to-DC converter topologies.

BUCK CONVERTER STEP-DOWN CONVERTER

In this circuit the transistor turning ON will put voltage V_{in} on one end of the inductor. This voltage will tend to cause the inductor current to rise. When the transistor is OFF, the current will continue flowing through the inductor but now flowing through the diode.

We initially assume that the current through the inductor does not reach zero, thus the voltage at V_x will now be only the voltage across the conducting diode during the full OFF time. The average voltage at V_x will depend on the average ON time of the transistor provided the inductor current is continuous.

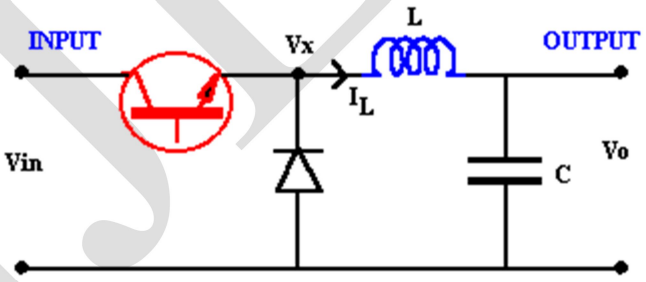

Buck Converter

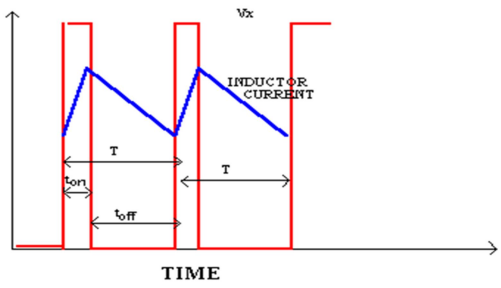

Voltage and current changes

To analyze the voltages of this circuit let us consider the changes in the inductor current over one cycle. From the relation

$$V_x - V_o = L\frac{di}{dt} \quad \ldots\ldots\ldots\ldots\ldots\ldots (1)$$

The change of current satisfies

$$di = \int_{ON}(V_x - V_o)dt + \int_{OFF}(V_x - V_o)dt \quad \ldots\ldots\ldots (2)$$

For steady state operation the current at the start and end of a period T will not change. To get a simple relation between voltages we assume no voltage drop across transistor or diode while ON and a perfect switch change. Thus during the ON time $V_x=V_{in}$ and in the OFF $V_x=0$. Thus

$$0 = di = \int_0^{t_{on}}(Vin - Vo)dt + \int_{t_{on}}^{t_{on}+t_{off}}(-Vo)dt \quad \ldots\ldots\ldots\ldots\ldots\ldots (3)$$

Which simplifies to

$$(Vin - Vo)t_{on} - Vo\ t_{off} = 0 \quad \ldots\ldots\ldots\ldots (4)$$

or

$$\frac{Vo}{Vin} = \frac{t_{on}}{T} \quad \ldots\ldots\ldots\ldots (5)$$

And defining "duty ratio" as

$$D = \frac{t_{on}}{T} \quad \ldots\ldots\ldots (6)$$

The voltage relationship becomes Vo=D Vin Since the circuit is lossless and the input and output powers must match on the average $V_o * I_o = V_{in} * I_{in}$. Thus the average input and output current must satisfy $I_{in} = D\ I_o$ These relations are based on the assumption that the inductor current does not reach zero.

CUK CONVERTER

The buck, boost and buck-boost converters all transferred energy between input and output using the inductor, analysis is based of voltage balance across the inductor. The CUK

converter uses capacitive energy transfer and analysis is based on current balance of the capacitor. The circuit in Fig. below(CUK converter) is derived from DUALITY principle on the buck-boost converter.

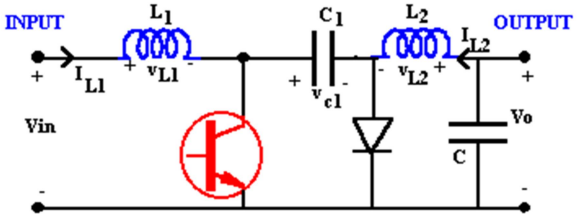

CUK Converter

If we assume that the current through the inductors is essentially ripple free we can examine the charge balance for the capacitor C1. For the transistor ON the circuit becomes

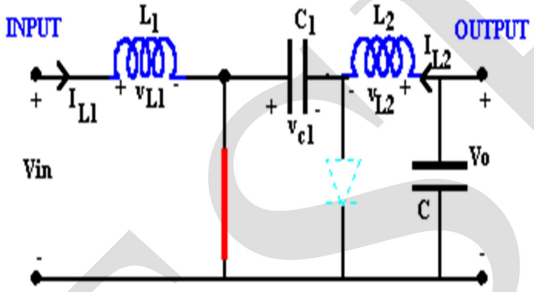

CUK "ON-STATE"

And the current in C1 is I_{L1}. When the transistor is OFF, the diode conducts and the current in C1 becomes I_{L2}.

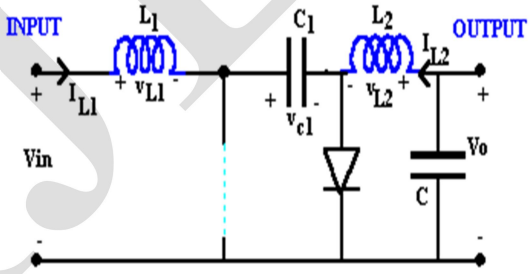

CUK "OFF-STATE"

Since the steady state assumes no net capacitor voltage rise ,the net current is zero

$$I_{L1} t_{ON} + (-I_{L2}) t_{OFF} = 0 \quad \text{..... (24)}$$

Which implies

$$\frac{I_{L2}}{I_{L1}} = \frac{(1-D)}{D} \quad \text{..... (25)}$$

The inductor currents match the input and output currents, thus using the power conservation rule

$$\frac{Vo}{Vin} = -\frac{D}{(1-D)} \quad \ldots\ldots\ldots\ldots (26)$$

Thus the voltage ratio is the same as the buck-boost converter. The advantage of the CUK converter is that the input and output inductors create a smooth current at both sides of the converter while the buck, boost and buck-boost have at least one side with pulsed current.

Isolated DC-DC Converters

In many DC-DC applications, multiple outputs are required and output isolation may need to be implemented depending on the application. In addition, input to output isolation may be required to meet safety standards and / or provide impedance matching.

The above discussed DC-DC topologies can be adapted to provide isolation between input and output.

Flyback Converter

The flyback converter can be developed as an extension of the Buck-Boost converter. Fig (a) shows the basic converter; Fig (b)(replacing inductor by transformer) replaces the inductor by a transformer. The buck-boost converter works by storing energy in the inductor during the ON phase and releasing it to the output during the OFF phase. With the transformer the energy storage is in the magnetization of the transformer core. To increase the stored energy a gapped core is often used.

In Fig (c) the isolated output is clarified by removal of the common reference of the input and output circuits.

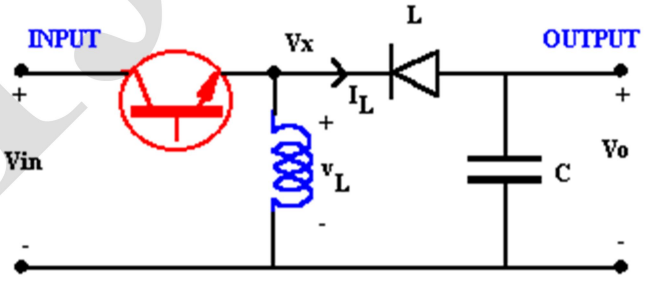

(a) Buck-Boost Converter

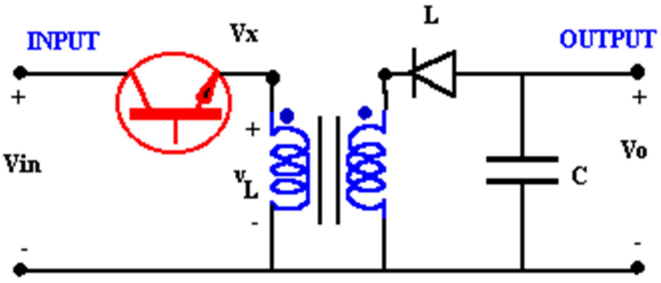

(b) Replacing inductor by transformer

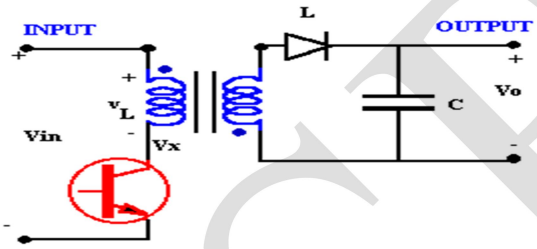

(c) Flyback converter re-configured

Forward Converter

The concept behind the forward converter is that of the ideal transformer converting the input AC voltage to an isolated secondary output voltage. For the circuit in Fig. (forward converter), when the transistor is ON, Vin appears across the primary and then generates

$$Vx = \frac{N_1}{N_2} Vin \quad \ldots\ldots\ldots\ldots (27)$$

The diode D1 on the secondary ensures that only positive voltages are applied to the output circuit while D2 provides a circulating path for inductor current if the transformer voltage is zero or negative.

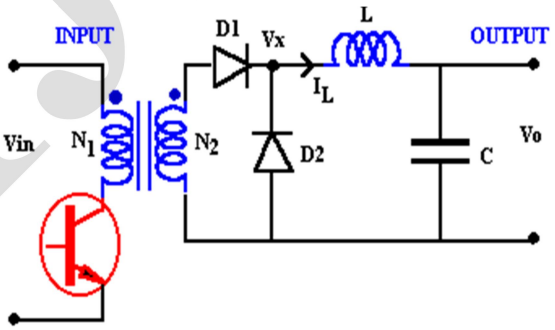

Forward Converter

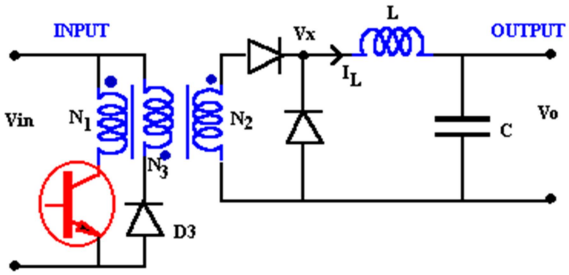

Forward converter with tertiary winding

MODELING OF CASE STUDY

SYSTEM CONFIGURATION AND MODELING:

A. Grid Configuration:

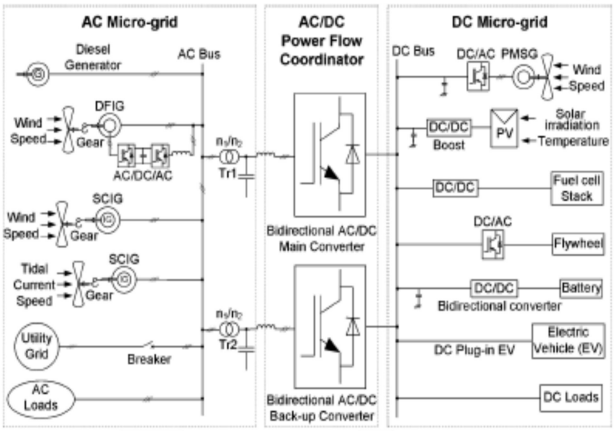

Fig.1. A hybrid ac/dc micro grid system.

Fig. 1 shows a conceptual hybrid system configuration where various ac and dc sources and loads are connected to the corresponding dc and ac networks. The ac and dc links are connected together through two transformers and two four-quadrant operating three phase converters. The ac bus of the hybrid grid is tied to the utility grid.

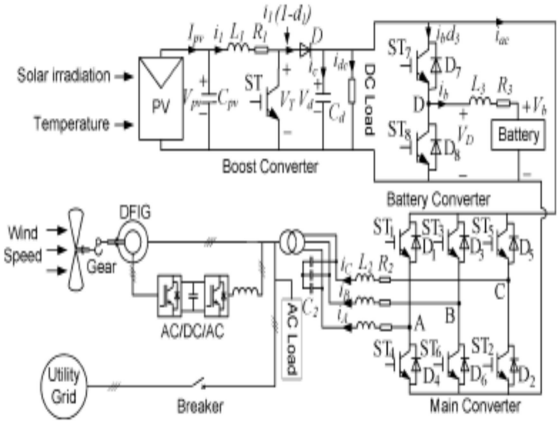

Fig. 2. A compact representation of the proposed hybrid grid.

A compact hybrid grid as shown in Fig. 2 is modeled using the Simulink in the MATLAB to simulate system operations and controls. Forty kW PV arrays are connected to dc

bus through a dc/dc boost converter to simulate dc sources. A capacitor C_{pv} is to suppress high frequency ripples of the PV output voltage.

A 50 kW wind turbine generator (WTG) with doubly fed induction generator (DFIG) is connected to an ac bus to simulate ac sources. A 65 Ah battery as energy storage is connected to dc bus through a bidirectional dc/dc converter. Variable dc load (20 kW–40 kW) and ac load (20 kW–40 kW) are connected to dc and ac buses respectively. The rated voltages for dc and ac buses are 400 V and 400 V rms respectively. A three phase bidirectional dc/ac main converter with R-L-C filter connects the dc bus to the ac bus through an isolation transformer.

B. Grid Operation:

The hybrid grid can operate in two modes. In grid-tied mode, the main converter is to provide stable dc bus voltage and required reactive power and to exchange power between the ac and dc buses. The boost converter and WTG are controlled to provide the maximum power. When the output power of the dc sources is greater than the dc loads, the converter acts as an inverter and injects power from dc to ac side. When the total power generation is less than the total load at the dc side, the converter injects power from the ac to dc side. When the total power generation is greater than the total load in the hybrid grid, it will inject power to the utility grid. Otherwise, the hybrid grid will receive power from the utility grid. In the grid tied mode, the battery converter is not very important in system operation because power is balanced by the utility grid.

In autonomous mode, the battery plays a very important role for both power balance and voltage stability. Control objectives for various converters are dispatched by energy management system. DC bus voltage is maintained stable by a battery converter or boost converter according to different operating conditions. The main converter is controlled to provide a stable and high quality ac bus voltage. Both PV and WTG can operate on maximum power point tracking (MPPT) or off-MPPT mode based on system operating requirements. Variable wind speed and solar irradiation are applied to the WTG and PV arrays respectively to simulate variation of power of ac and dc sources and test the MPPT control algorithm.

C. Modeling of PV Panel:

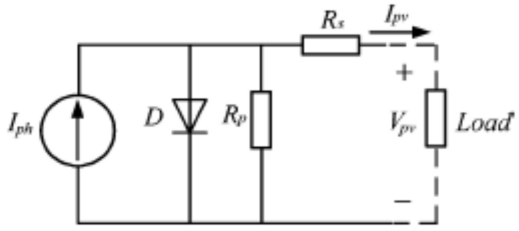

Fig. 3. Equivalent circuit of a solar cell.

Fig. 3 shows the equivalent circuit of a PV panel with a load. The current output of the PV panel is modeled by the following three equations. All the parameters are shown in Table I:

TABLE I
PARAMETERS FOR PHOTOVOLTAIC PANEL

Symbol	Description	Value
V_{oc}	Rated open circuit voltage	403 *V*
I_{ph}	Photocurrent	
I_{sat}	Module reverse saturation current	
q	Electron charge	1.602×10^{-19} *C*
A	Ideality factor	1.50
k	Boltzman constant	1.38×10^{-23} *J/K*
R_s	Series resistance of a PV cell	
R_p	parallel resistance of a PV cell	
I_{sso}	Short-circuit current	3.27 *A*
k_i	SC current temperature coefficient	$1.7e^{-3}$
T_r	Reference temperature	301.18 *K*
I_{rr}	Reverse saturation current at T_r	$2.0793e^{-6}$ *A*
E_{gap}	Energy of the band gap for silicon	1.1*eV*
n_p	Number of cells in parallel	40
n_s	Number of cells in series	900
S	Solar radiation level	0~1000 W/m^2
T	Surface temperature of the PV	350 *K*

$$I_{pv} = n_p I_{ph} - n_p I_{\text{sat}} \times \left[\exp\left(\left(\frac{q}{AkT}\right)\left(\frac{V_{pv}}{n_s} + I_{pv}R_s\right)\right) - 1\right] \quad (1)$$

$$I_{ph} = (I_{sso} + k_i(T - T_r)) \cdot \frac{S}{1000} \quad (2)$$

$$I_{\text{sat}} = I_{rr}\left(\frac{T}{T_r}\right)^3 \exp\left(\left(\frac{qE_{\text{gap}}}{kA}\right) \cdot \left(\frac{1}{T_r} - \frac{1}{T}\right)\right) \quad (3)$$

D. Modeling of Battery:

Two important parameters to represent state of a battery are terminal voltage v_b and state of charge (SOC) as follows

$$V_b = V_o + R_b \cdot i_b - K\frac{Q}{Q + \int i_b dt} + A \cdot \exp\left(B \int i_b dt\right) \quad (4)$$

$$\text{SOC} = 100\left(1 + \frac{\int i_b dt}{Q}\right) \quad (5)$$

Where R_b is internal resistance of the battery, V_o is the open circuit voltage of the battery, i_b is battery charging current, K is polarization voltage, Q is battery capacity, A is exponential voltage, B and is exponential capacity.

E. Modeling of Wind Turbine Generator:

Power output P_m from a WTG is determined by (6)

$$P_m = 0.5\rho A C_p(\lambda, \beta) V_w^3 \quad (6)$$

Where ρ is air density, A is rotor swept area, V_ω is wind speed, and $C_p(\lambda, \beta)$ is the power coefficient, which is the function of tip speed ratio λ and pitch angle β.

The mathematical models of a DFIG are essential requirement for its control system. The voltage equations of an induction motor in a rotating *d-q* coordinate are as follows:

$$\begin{bmatrix} u_{ds} \\ u_{qs} \\ u_{dr} \\ u_{qr} \end{bmatrix} = \begin{bmatrix} -R_s & 0 & 0 & 0 \\ 0 & -R_s & 0 & 0 \\ 0 & 0 & R_r & 0 \\ 0 & 0 & 0 & R_r \end{bmatrix} \begin{bmatrix} i_{ds} \\ i_{qs} \\ i_{dr} \\ i_{qr} \end{bmatrix} + p \begin{bmatrix} \lambda_{ds} \\ \lambda_{qs} \\ \lambda_{dr} \\ \lambda_{qr} \end{bmatrix} + \begin{bmatrix} -\omega_1 \lambda_{qs} \\ \omega_1 \lambda_{ds} \\ -\omega_2 \lambda_{qr} \\ \omega_2 \lambda_{dr} \end{bmatrix} \quad (7)$$

$$\begin{bmatrix} \lambda_{ds} \\ \lambda_{qs} \\ \lambda_{dr} \\ \lambda_{qr} \end{bmatrix} = \begin{bmatrix} -L_s & 0 & L_m & 0 \\ 0 & -L_s & 0 & L_m \\ -L_m & 0 & L_r & 0 \\ 0 & -L_m & 0 & L_r \end{bmatrix} \begin{bmatrix} i_{ds} \\ i_{qs} \\ i_{dr} \\ i_{qr} \end{bmatrix} \quad (8)$$

The dynamic equation of the DFIG

$$\frac{J}{n_p}\frac{d\omega_r}{dt} = T_m - T_{em} \quad (9)$$

$$T_{em} = n_p L_m (i_{qs} i_{dr} - i_{ds} i_{qr}) \quad (10)$$

Where the subscripts *d, q ,s*, and denote d-axis, q-axis, stator, and rotor respectively, L represents the inductance, is the flux linkage, *u* and *i* represent voltage and current respectively,ω_1 and ω_2 are the angular synchronous speed and slip speed respectively, $\omega_2 = \omega_1 - \omega_r$,T_m is the mechanical torque, T_{em} is the electromagnetic torque and other parameters of DIFG are listed in Table II.

If the synchronous rotating - reference is oriented by the stator voltage vector, the -axis is aligned with the stator voltage vector while the -axis is aligned with the stator flux reference frame. Therefore, $\lambda_{ds}=0$ and $\lambda_{qs}= \lambda_s$. The following equations can be obtained in the stator voltage oriented reference frame as

$$i_{ds} = -\frac{L_m}{L_s} i_{dr} \quad T_{em} = n_p \frac{L_m}{L_s} \lambda_s i_{dr}$$

$$\sigma = \frac{L_s L_r - L_m^2}{L_s L_r} \quad (11)$$

$$u_{dr} = R_r i_{dr} + \sigma L_r \frac{di_{dr}}{dt} - (\omega_1 - \omega_r)(L_m i_{qs} + L_r i_{qr}) \quad (12)$$

$$u_{qr} = R_r i_{qr} + \sigma L_r \frac{di_{qr}}{dt} + (\omega_1 - \omega_r)(L_m i_{ds} + L_r i_{dr}) \quad (13)$$

COORDINATION CONTROL OF THE CONVERTERS:

There are five types of converters in the hybrid grid. Those converters have to be coordinately controlled with the utility grid to supply an uninterrupted, high efficiency, and high quality power to variable dc and ac loads under variable solar irradiation and wind speed when the hybrid grid operates in both isolated and grid tied modes. The control algorithms for those converters are presented in this section.

A. Grid-Connected Mode:

When the hybrid grid operates in this mode, the control objective of the boost converter is to track the MPPT of the PV array by regulating its terminal voltage. The back-to-back ac/dc/ac converter of the DFIG is controlled to regulate rotor side current to achieve MPPT and to synchronize with ac grid. The energy surplus of the hybrid grid can be sent to the utility system. The role of the battery as the energy storage becomes less important because the power is balanced by the utility grid. In this case, the only function of the battery is to eliminate frequent power transfer between the dc and ac link. The dc/dc converter of the battery can be controlled as the energy buffer using the technique. The main converter is designed to operate bidirectionally

to incorporate complementary characteristic of wind and solar sources. The control objectives of the main converter are to maintain a stable dc-link voltage for variable dc load and to synchronize with the ac link and utility system.

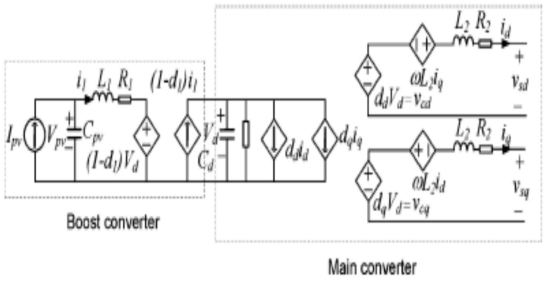

Fig. 4. Time average model for the booster and main converter.

The combined time average equivalent circuit model of the booster and main converter is shown in Fig. 4 based on the basic principles and description for booster and inverter respectively.

Power flow equations at the dc and ac links are as follows:

$$P_{pv} + P_{ac} = P_{dcL} + P_b \tag{14}$$

$$P_s = P_w - P_{acL} - P_{ac} \tag{15}$$

Where real power P_{pv} and P_w are produced by PV and WTG respectively, P_{acL} and P_{dcL} are real power loads connected to ac and dc buses respectively, P_{ac} is the power exchange between ac and dc links, P_b is power injection to battery, and P_s is power injection from the hybrid grid to the utility.

The current and voltage equations at dc bus are as follows:

$$V_{pv} - V_T = L_1 \cdot \frac{di_1}{dt} + R_1 i_1 \tag{16}$$

$$I_{pv} - i_1 = C_{pv} \cdot \frac{dV_{pv}}{dt} \tag{17}$$

$$V_T = V_d \cdot (1 - d_1) \tag{18}$$

$$i_1 (1 - d_1) - C_d \frac{dV_d}{dt} - \frac{1}{R_L} V_d - i_b - i_{ac} = 0 \tag{19}$$

Where d_1 is the duty ratio of switch ST.

Equations (20) and (21) show the ac side voltage equations of the main converter in ABC and d- q coordinates respectively.

$$L_2\frac{d}{dt}\begin{bmatrix} i_A \\ i_B \\ i_C \end{bmatrix} + R_2\begin{bmatrix} i_A \\ i_B \\ i_C \end{bmatrix} = \begin{bmatrix} v_{CA} \\ v_{CB} \\ v_{CC} \end{bmatrix} - \begin{bmatrix} v_{SA} \\ v_{SB} \\ v_{SC} \end{bmatrix} \quad (20)$$

$$L_2\frac{d}{dt}\begin{bmatrix} i_d \\ i_q \end{bmatrix} = \begin{bmatrix} -R_2 & \omega L_2 \\ -\omega L_2 & -R_2 \end{bmatrix}\begin{bmatrix} i_d \\ i_q \end{bmatrix} + \begin{bmatrix} v_{cd} \\ v_{cq} \end{bmatrix} - \begin{bmatrix} v_{sd} \\ v_{sq} \end{bmatrix} \quad (21)$$

Where (v_{CA}, v_{CB}, v_{CC}) are ac side voltages of the main converter, (v_{SA}, v_{SB}, v_{SC}) are voltages across in Fig. 2, and $(i_d, i_q), (v_{sd}, v_{sq},)$, and (v_{cd}, v_{cq}) are the corresponding d-q coordinate variables.

In order to maintain stable operation of the hybrid grid under various supply and demand conditions, a coordination control algorithm for booster and main converter is proposed based on basic control algorithms of the grid interactive inverter. The control block diagram is shown in Fig. 5.

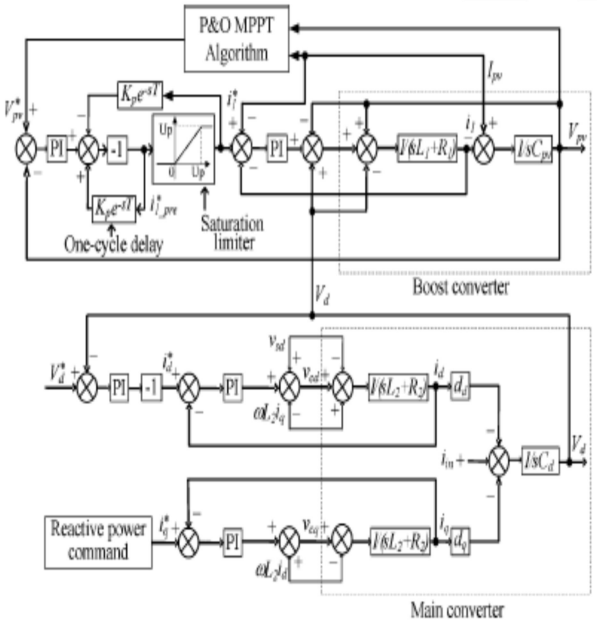

Fig. 5. The control block diagram for boost converter and main converter.

The reference value of the solar panel terminal voltage is determined by the basic perturbation and observation (P&O) algorithm based on solar irradiation and temperature to harness the maximum power. Dual-loop control for the dc/dc boost converter is described, where the control objective is to provide a high quality dc voltage with good dynamic response. This control scheme is applied for the PV system to track optimal solar panel terminal voltage using the MPPT algorithm with minor modifications. The outer voltage loop can guarantee voltage reference tracking with zero steady-state error and the inner current loop can improve dynamic response.

The one-cycle delay and saturation limiter in Fig. 5 can assist controller to track V_{pv}^* faster. In steady state, $i_1^*{}_{-pre}$ resides in the linear region of the saturation limiter and is equal to i_1^*. It can be seen that a step increase of V_{pv}^* makes $i_1^*{}_{-pre}$ becomes negative, which in turn makes i_1^* to be zero during the first switching period of the transient process.

This leads to a lower d_1 for driving the average voltage $V_d(1-d_1)$ and V_{pv} upward to follow the V_{pv}^* command.

To smoothly exchange power between dc and ac grids and supply a given reactive power to the ac link, PQ control is implemented using a current controlled voltage source for the main converter. Two PI controllers are used for real and reactive power control respectively. When resource conditions or load capacities change, the dc bus voltage is adjusted to constant through PI regulation. The PI controller is set as instantaneous active current i_d reference whereas the instantaneous reactive current i_q reference is determined by reactive power compensation command.

When a sudden dc load drop causes power surplus at dc side, the main converter is controlled to transfer power from the dc to the ac side. The active power absorbed by capacitor C_d leads to the rising of dc-link voltage V_d. The negative error $(V_d^* - V_d)$ caused by the increase of V_d produces a higher active current reference i_d^* through the PI control. The active current and its reference i_d^* are both positive. A higher positive reference i_d^* will force active current i_d to increase through the inner current control loop. Therefore, the power surplus of the dc grid can be transferred to the ac side.

Similarly, a sudden increase of dc load causes the power shortage and V_d drop at the dc grid. The main converter is controlled to supply power from the ac to the dc side. The positive voltage error $(V_d^* - V_d)$ caused by V_d drop makes the magnitude of i_d^* increase through the PI control. Because i_d and i_d^* are both negative, the magnitude of i_d is increased through the inner current control loop. Therefore, power is transferred from the ac grid to the dc side.

The DFIG is controlled to maintain a stable dc-link voltage of the back-to-back ac/dc/ac converter. The objectives of the rotor side converter are to track MPPT of the WTG and to manage the stator side reactive power. Different control schemes such as the direct torque control (DTC) and direct power control (DPC) have been proposed for a DFIG. The DTC scheme as shown in Fig. 6 is selected as the control method for the rotor side converter in this paper. The rotor rotational speed is obtained through the MPPT algorithm, which is based on the power and speed characteristic of the wind turbine. The rotational speed ω_r and mechanical power P_m are used to calculate the electromagnetic torque T_{em}^*.

The –axis rotor side current reference is determined based on T_{em}^* through stator flux estimation. The rotor side *d-q* voltages are maintained through controlling the corresponding current with appropriate feed forward voltage compensation.

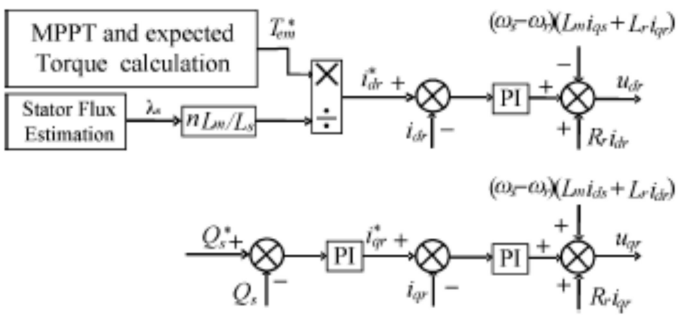

Fig. 6. The DTC control scheme for the rotor side converter.

B. Isolated Mode:

When the hybrid grid operates in the islanding mode, the boost converter and the back-to-back ac/dc/ac converter of the DFIG may operate in the on-MPPT or off-MPPT based on system power balance and energy constraints. The main converter acts as a voltage source to provide a stable voltage and frequency for the ac grid and operates either in inverter or converter mode for the smooth power exchange between ac and dc links. The battery converter operates either in charging or discharging mode based on power balance in the system. The dc-link voltage is maintained by either the battery or the boost converter based on system operating condition. Powers under various load and supply conditions should be balanced as follows:

$$P_{pv} + P_w = P_{acL} + P_{dcL} + P_{\text{loss}} + P_b \tag{22}$$

Where P_{loss} is the total grid loss.

Two level coordination controls are used to maintain system stable operation. At the system level, operation modes of the individual converters are determined by the energy management system (EMS) based on the system net power P_{net} and the energy constraints and the charging/discharging rate of battery. The system control logic diagram is shown in Fig. 7. P_{net} is defined as the total maximum power generation minus the total load and minus P_{loss}. The energy constraints of the battery are determined based on the state of charge (SOC) limits using $\text{SOC}_{\min} < \text{SOC} \leq \text{SOC}_{\max}$. It should be noted that SOC cannot be measured directly, but can be attained through some estimation methods as described.

The constraint of charging and discharging rate is $P_b \leq P_{b\max}$. At local level, the individual converters operate based on mode commends from the EMS. Either the PV system or WTG or both have to operate in the off-MPPT mode for Case 1 and Case 2 and in the on-MPPT mode for other cases. The battery converter may operate in the idle, charging, or discharging mode for different cases. The main converter will operate in the inverter mode if $P_w - P_{acL}$ is negative or in the converter mode with positive $P_w - P_{acL}$. Load shedding is required to maintain power balance if power supply is less than demand and the battery is at the minimum SOC.

Fig.7. Control mode diagram for the isolated hybrid grid.

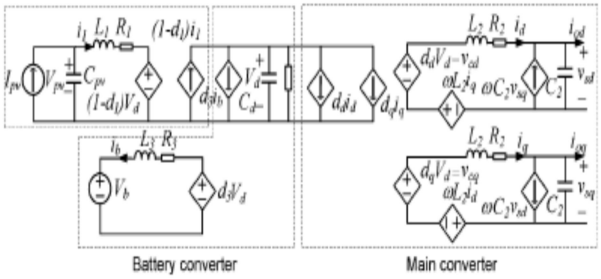

Fig. 8. Time average equivalent circuit model for the three converters.

The time average equivalent circuit model of the booster, main converter, and battery converter for the isolated operation is shown in Fig. 8. The inverter part of the circuit model in Fig. 8 is based on the basic principles and descriptions. The current and voltage equations for the battery converter and dc link are as follows:

$$V_D - V_b = L_3 \cdot \frac{di_b}{dt} + R_3 i_b \quad (23)$$

$$V_D = V_d \cdot d_3 \quad (24)$$

$$i_1(1-d_1) - i_{ac} - i_{dc} - i_b \cdot d_3 = i_c = C_d \cdot \frac{dV_d}{dt} \quad (25)$$

Where d_3 and $(1-d_3)$ are the duty ratio of the switches ST_7 and ST_8 respectively. The ac side current equations of the main converter in *d-q* coordinate are as follows:

$$C_2 \frac{d}{dt}\begin{bmatrix} v_{sd} \\ v_{sq} \end{bmatrix} = \begin{bmatrix} i_d \\ i_q \end{bmatrix} + \begin{bmatrix} 0 & \omega \\ -\omega & 0 \end{bmatrix}\begin{bmatrix} v_{sd} \\ v_{sq} \end{bmatrix} - \begin{bmatrix} i_{od} \\ i_{oq} \end{bmatrix} \quad (26)$$

Where i_{od} and i_{oq} are *d-q* currents at the converter side of the transformer respectively.

Multi-loop voltage control for a dc/ac inverter is described, where the control objective is to provide a high quality ac voltage with good dynamic response at different load conditions. This control scheme can also be applied for main converter control to provide high quality ac voltage in stand-alone mode with minor modifications. The coordinated control block diagram for the normal case is shown in Fig. 9. To provide a stable dc-link voltage, the dual loop control scheme is applied for the battery converter. The injection current $I_{in} = i_1(1-d_1) - i_{ac} - i_{dc}$. It should be noted that the output of the outer voltage loop is multiplied by -1 before it is set as the inner loop current reference.

Current i_b is defined positive when flowing into the battery, where the preset dc-link voltage V_{dc}^* is set to constant 400 V. Considering a decrease of V_{dc} caused by sudden load increase or decrease of solar irradiation, the positive voltage error $(V_{dc}^* - V_{dc})$ multiplied by through the PI produces a negative i_b^* for the inner current loop, which makes the battery to transfer from charging into discharging mode and to rise V_{dc} back to its preset value V_{dc}^*. The battery converter is transferred from discharging into charging mode in the similar control method. The main converter provides a stable ac bus voltage for the DFIG converter as shown in the bottom of Fig. 9.

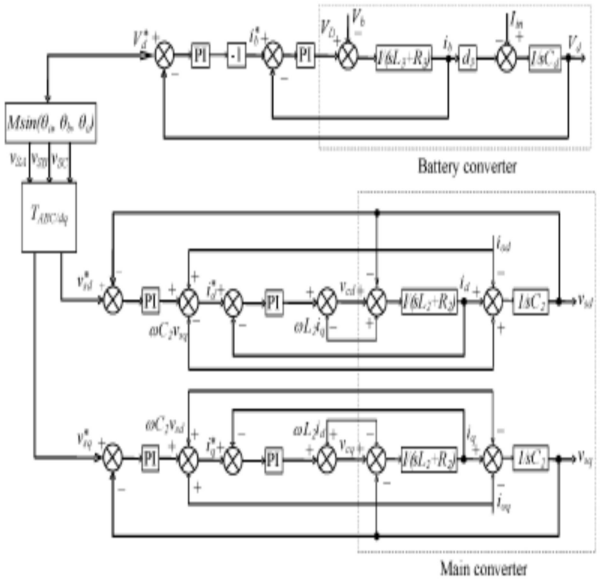

Fig. 9. Block diagram of the battery and main converters for the normal case.

The control objectives for the converters change when the system transfers from one operating scenario to another. For example, the role of the boost converter is changed to provide a stable dc-link voltage rather than the MPPT for cases 1 and 2, while the battery converter is controlled to absorb the maximum power in case 1 and is switched off in case 2. The coordinated control block diagram for these two converters in Case 1 is described in Fig. 10. The boost converter provides a stable dc-link voltage. The main converter is controlled to provide a stable ac bus voltage. The current I_{o} in Fig. 10 is equal to $i_{ac}+i_{dc}+i_{b}d_{3}$ and d'_{1} is equal to $(1-d_1)$.

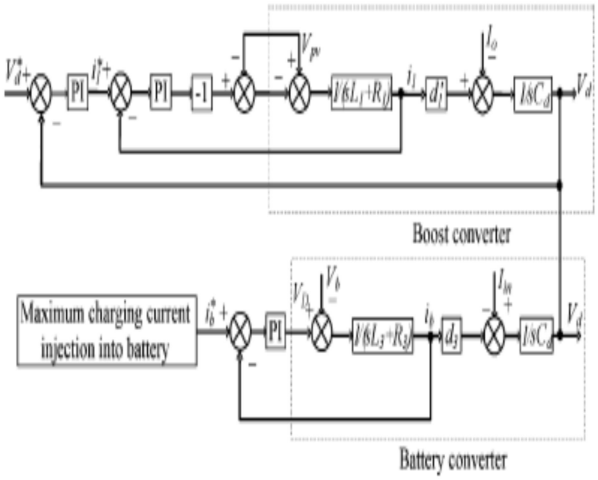

Fig.10. Block diagram of the booster and battery converter for Case 1.

The anti-islanding technique is one of the essential functions for reliable operation of distributed generation systems. Many anti-islanding detection and control schemes have been developed for conventional and power-converter-based distributed generators and various micro grids. Those techniques can be modified and implemented in the proposed hybrid grid to make the system transfer smoothly from the grid tied to isolated mode.

MATLAB DESIGN OF CASE STUDY & RESULTS

Main circuit

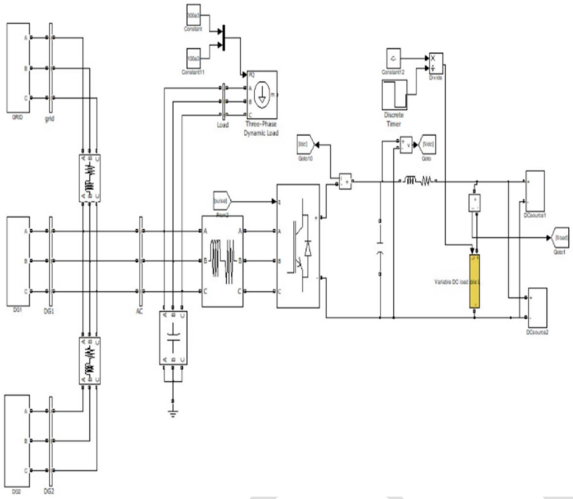

Control circuit

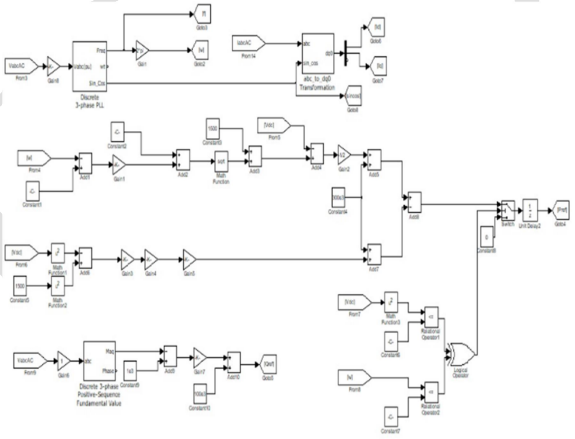

Generating station

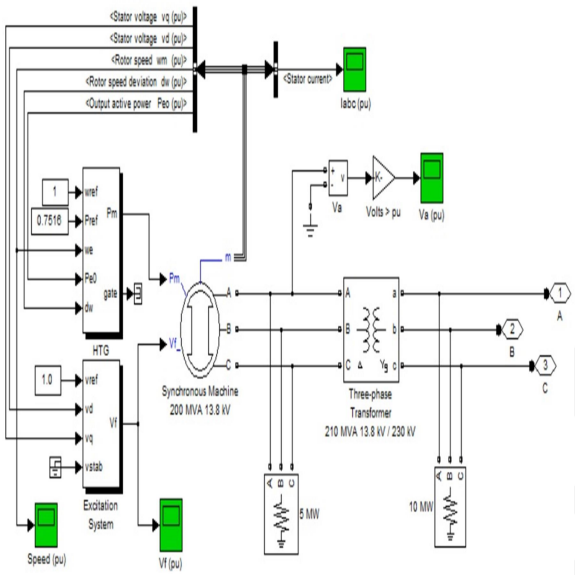

Renewable energy source

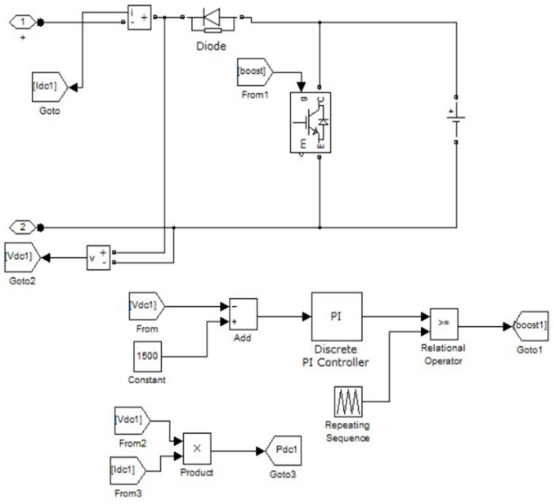

Power and voltage graphs

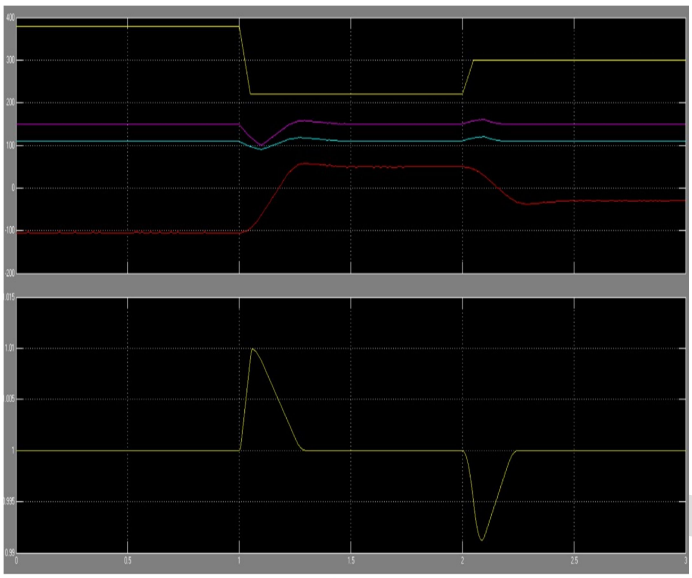

CONCLUSION

A hybrid ac/dc micro grid is proposed and comprehensively studied in this paper. The models and coordination control schemes are proposed for the all the converters to maintain stable system operation under various load and resource conditions. The coordinated control strategies are verified by MATLAB/Simulink. Various control methods have been incorporated to harness the maximum power from dc and ac sources and to coordinate the power exchange between dc and ac grid. Different resource conditions and load capacities are tested to validate the control methods. The simulation results show that the hybrid grid can operate stably in the grid-tied or isolated mode. Stable ac and dc bus voltage can be guaranteed when the operating conditions or load capacities change in the two modes. The power is smoothly transferred when load condition changes.

Although the hybrid grid can reduce the processes of dc/ac and ac/dc conversions in an individual ac or dc grid, there are many practical problems for implementing the hybrid grid based on the current ac dominated infrastructure. The total system efficiency depends on the reduction of conversion losses and the increase for an extra dc link. It is also difficult for companies to redesign their home and office products without the embedded ac/dc rectifiers although it is theoretically possible. Therefore, the hybrid grids may be implemented when some small customers want to install their own PV systems on the roofs and are willing to use LED lighting systems and EV charging systems. The hybrid grid may also be feasible for some small isolated industrial plants with both PV system and wind turbine generator as the major power supply.

REFERENCES

[1] R. H. Lasseter, “Micro Grids,” in Proc. IEEE Power Eng. Soc. Winter Meet., Jan. 2002, vol. 1, pp. 305–308.

[2] Y. Zoka, H. Sasaki, N. Yorino, K. Kawahara, and C. C. Liu, "An interaction problem of distributed generators installed in a Micro Grid," in Proc. IEEE Elect. Utility Deregulation, Restructuring. Power Technol., Apr. 2004, vol. 2, pp. 795–799.

[3] R. H. Lasseter and P. Paigi, "Micro grid: A conceptual solution," in Proc. IEEE 35th PESC, Jun. 2004, vol. 6, pp. 4285–4290.

[4] C. K. Sao and P. W. Lehn, "Control and power management of converter fed Micro Grids," IEEE Trans. Power Syst., vol. 23, no. 3, pp. 1088–1098, Aug. 2008.

[5] T. Logenthiran, D. Srinivasan, and D.Wong, "Multi-agent coordination for DER in Micro Grid," in Proc. IEEE Int. Conf. Sustainable Energy Technol., Nov. 2008, pp. 77–82.

[6] M. E. Baran and N. R. Mahajan, "DC distribution for industrial systems: Opportunities and challenges," IEEE Trans. Ind. Appl., vol. 39, no. 6, pp. 1596–1601, Nov. 2003.

[7] Y. Ito, Z.Yang, and H. Akagi, "DC micro-grid based distribution power generation system," in Proc. IEEE Int. Power Electron. Motion Control Conf., Aug. 2004, vol. 3, pp. 1740–1745.

[8] A. Sannino, G. Postiglione, and M. H. J. Bollen, "Feasibility of a DC network for commercial facilities," IEEE Trans. Ind. Appl., vol. 39, no. 5, pp. 1409–1507, Sep. 2003.

[9] D. J. Hammerstrom, "AC versus DC distribution systems-did we get it right?," in Proc. IEEE Power Eng. Soc. Gen. Meet., Jun. 2007, pp. 1–5.

[10] D. Salomonsson and A. Sannino, "Low-voltage DC distribution system for commercial power systems with sensitive electronic loads," IEEE Trans. Power Del., vol. 22, no. 3, pp. 1620–1627, Jul. 2007.

[11] M. E. Ropp and S. Gonzalez, "Development of a MATLAB/Simulink model of a single-phase grid-connected photovoltaic system," IEEE Trans. Energy Conv., vol. 24, no. 1, pp. 195–202, Mar. 2009.

[12] K. H. Chao, C. J. Li, and S. H. Ho, "Modeling and fault simulation of photovoltaic generation systems using circuit-based model," in Proc. IEEE Int. Conf. Sustainable Energy Technol., Nov. 2008, pp. 290–294.